N-89
397 234

EVALUATION AND SELECTION OF REPLACEMENT THERMAL CONTROL MATERIALS FOR THE HUBBLE SPACE TELESCOPE

Jacqueline A. Townsend, Patricia A. Hansen, Mark W. McClendon,
NASA Goddard Space Flight Center, Greenbelt, Maryland, 20771 USA

Joyce A. Dever
NASA Lewis Research Center, Cleveland, Ohio 44135 USA

Jack. J. Triolo
Swales Aerospace, Beltsville, Maryland 20705 USA

ABSTRACT

The mechanical and optical properties of the metallized Teflon® FEP thermal control materials on the Hubble Space Telescope (HST) have degraded over the nearly seven years the telescope has been in orbit. Given the damage to the outer layer of the multi-layer insulation (MLI) that was apparent during the second servicing mission (SM2), the decision was made to replace the outer layer during subsequent servicing missions. A Failure Review Board was established to investigate the damage to the MLI and identify a replacement material. The replacement material had to meet the stringent thermal requirements of the spacecraft and maintain structural integrity for at least ten years.

Ten candidate materials were selected and exposed to ten-year HST-equivalent doses of simulated orbital environments. Samples of the candidates were exposed sequentially to low and high energy electrons and protons, atomic oxygen, x-ray radiation, ultraviolet radiation and thermal cycling. Following the exposures, the mechanical integrity and optical properties of the candidates were investigated using Optical Microscopy, Scanning Electron Microscopy (SEM), and a Laboratory Portable Spectroreflectometer (LPSR). Based on the results of these simulations and analyses, the FRB selected a replacement material and two alternates that showed the highest likelihood of providing the requisite thermal properties and surviving for ten years in orbit.

KEY WORDS: Low Earth Orbit (LEO) Simulated Environments, Teflon® FEP (fluorinated ethylene propylene), Thermal Control Materials

1. INTRODUCTION

The Hubble Space Telescope (HST) was launched into low Earth orbit (LEO) in April 1990 with Multi-Layer Insulation (MLI) blankets on the Light Shield (LS), Forward Shell (FS), and several Equipment Bays (1). The outer layer of these multi-layer blankets was aluminized Teflon® FEP (fluorinated ethylene propylene). Following the First Servicing Mission (SM1) in December 1993, analysis of retrieved MLI blankets revealed that the outer layer was beginning to degrade (3). When astronauts returned for the Second Servicing Mission (SM2) in February 1997, they discovered severe cracking in the outer layer of the MLI blankets on both solar facing and anti-

solar facing surfaces of HST. A small specimen of the outer layer was retrieved from the LS region and returned for ground-based analysis (1, 2).

Testing of the MLI specimen that was returned during SM2 revealed that the cracks observed on HST were a form of slow crack growth, which meant that they occurred slowly, under low stress, in the presence of a degrading environmental factor (2, 5). The Teflon® FEP had completely lost plastic deformation capability, indicating that significant chain scission had occurred (2). The material also showed an increased density and crystallinity (2, 9). The solar absorptance of the Teflon® FEP had increased due to bulk changes in the Teflon® FEP and cracking in the vapor deposited aluminum (VDA) backing (2, 7, 11, 13). This damage appeared to be the result of the combination of bulk damage from radiation exposure (electrons and protons) and the nearly 40,000 thermal cycles (-100 to +50 °C) the MLI experienced.

Given the severity of the damage, HST management decided it was likely that repairs to the outer layer would be required during the next servicing mission (SM3) in December, 1999. A Failure Review Board (FRB) was tasked to recommend a replacement material to be deployed during SM3 on the LS that would last through the spacecraft end-of-life (EOL) in 2010. The recommended material was required to maintain structural integrity over the course of ten years and have an EOL solar absorptance over hemispherical emittance ratio (α/ε) of less than 0.28.

In order to find a replacement material, the FRB selected ten promising candidate materials and subjected them to simulations of the HST orbital environment. The effort involved facilities at Boeing Space Systems and three NASA centers: Marshall Space Flight Center (MSFC), Lewis Research Center (LeRC), and Goddard Space Flight Center (GSFC). Following these exposures, the specimens were evaluated at GSFC in terms of crack propagation and morphology and optical properties.

2. MATERIALS

2.1 Candidate Selection Process To determine which materials should be tested, the FRB assembled a list of seventeen possible replacement materials and established a list of performance criteria. These nine criteria are listed below:

1. Low solar absorptance/thermal emittance ratio $\alpha/\varepsilon \leq 0.28$ at EOL
2. Ability to maintain structural integrity
3. Compatibility with EVA installation
4. Tear resistance
5. Not a source of contamination
6. Commercial availability for SM3 mission
7. Has demonstrated record of long term in-space durability in LEO
8. Suitable to construct a functional outer layer
9. Stowability

As part of the selection process, evaluation criteria with appropriate weighting factors were developed and used in a multiplicative evaluation process to assess each candidate material. The multiplicative evaluation process had been developed external to NASA but used extensively by NASA Lewis Research Center's Electro-Physics Branch for strategic planning and prioritization activities. Board members scored each candidate material according to how well they believed it would meet each of the performance criteria. In doing so, the damage to the current Teflon® FEP material was considered along with the issues specific to each of the various candidate replacement materials. Scores from each board member for each criteria were used in the multiplicative evaluation formula to calculate an overall score for each material. Based on this process, the original list of seventeen possible candidates was pared down to six candidate replacement materials which were then exposed to simulated space environments. Following the simulations, the actual performances of these six materials were evaluated with respect to these same criteria and a final selection was made.

2.2 Candidates Ten candidate replacement materials were evaluated in simulated low Earth orbit environments. Through this work the numbers below were used to refer to the material.

1. 10 mil Teflon® FEP/VDS/Inconel/non-UV-darkening adhesive/Nomex® scrim
2. 5 mil Teflon® FEP/VDS/Inconel/adhesive/fiberglass scrim/adhesive/2 mil Kapton®
3. 10 mil Teflon® FEP/VDA/non-UV-darkening adhesive/Nomex® scrim
4. 5 mil Teflon® FEP/VDA/non-darkening adhesive/fiberglass scrim/adhesive/2 mil Kapton®
5. 5 mil Teflon® FEP/VDS/Inconel/non-UV-darkening adhesive/Nomex® scrim
6. 5 mil Teflon® FEP /VDA/non-UV-darkening adhesive/Nomex scrim
7. OCLI multi-layer oxide UV blocker/2 mil white Tedlar®
8. 5 mil Teflon® FEP/VDA (the current material)
9. $SiO_2/Al_2O_3/Ag/Al_2O_3$/4 mil stainless steel
0. Proprietary Teflon® FEP/AZ93 White Paint/Kapton®

The first six materials were chosen based on the selection process described in section 2.1. Given the stringent thermal requirements (EOL $\alpha/\varepsilon \leq .28$), the options for candidate replacement materials were limited. Metallized Teflon® FEP met those thermal requirements, and photos taken during SM2 revealed that bonded Teflon® FEP used on HST had maintained its structural integrity. Because of this, several versions of Teflon® FEP/VDA and /VDS (vapor deposited silver) bonded to a scrim were candidates.

Four additional materials were included in the testing for other reasons. The current material (material 8), was included to verify that the test procedure could produce damage similar to that observed in orbit. Material 7 was included because it was used on HST exterior surfaces in other applications, and HST management wanted to anticipate its performance. Materials 9 and 10 were included at the discretion of the FRB Chair. Since the materials chosen through the selection process were so similar, materials 9 and 10 were included so that fundamentally different materials were evaluated in the event that none of the first six was successful.

3. EXPERIMENTAL

Since there was no facility for simultaneous exposure to a LEO-equivalent environment, the specimens were exposed to several environmental factors sequentially. The order of the exposures was designed to cause the maximum damage. Since the cracks in the HST materials were a form of slow crack growth, it was necessary to provide both the environmental factor and low stress in each simulation. In orbit, the stress was most likely associated with the thermal cycling (2). Since the specimens could not be thermal cycled during exposures to other environmental factors, special holders were developed to hold the specimens at constant strain while they were exposed to electrons, protons and AO.

Four sets of the candidates were exposed to electrons and protons at one of two facilities: MSFC or Boeing Space Systems Radiation facility. Following the electron/proton exposure, two sets were exposed to atomic oxygen (AO), and then thermal cycled at GSFC. Two other sets were exposed to x-rays at LeRC and thermal cycling at either LeRC or GSFC. The fluence values for these exposures were based on the estimates of the HST environment found in reference 1 of this volume.

3.1 Specimen Preparation Samples of the candidates were procured from several different vendors. Specimens with VDA were purchased from Dunmore and were backed with their proprietary, non-UV-darkening, polyester adhesive. Specimens with VDS were purchased from Sheldahl and were backed with their proprietary, non-UV-darkening, polyester adhesive. Material 7 was obtained from GSFC stock, material 8 was supplied by Lockheed Martin Missiles and Space from current stock, and material 9 was manufactured in the Thermal Branch at GSFC. Material 0 was provided by its manufacturer, AZTek. Specimen preparation was done in the Materials Engineering Branch and the Thermal Branch at GSFC.

The full sheet of each candidate was cured according to the manufacturer's specifications. Some were vacuum baked for up to 24 hours; others were received fully cured. Then each sheet was cleansed with an extracted clean-room wipe soaked in analytical-grade isopropyl alcohol. The sheets were then wrapped around a 0.5 cm diameter dowel along two axes to pre-stress the metal backing. Specimens were then cut in five different sizes to accommodate the test fixture at each exposure facility (see Table 1). A microtome blade was used to cut the individual specimens with identical orientation from a single sheet of each candidate material. A new blade was used

for each material. Control specimens were cut at the same time and stored in a lab at GSFC. Witness specimens were also cut and traveled with the test specimens to each test site.

TABLE 1: SPECIMEN DIMENSIONS

Specimen Set	Materials	Dimensions (length x width, cm)
M1	Candidates	12.7 x 1.27
M2	Candidates	12.7 x 1.27
M3	5 mil Teflon™ FEP/VDA	12.7 x 5.08
B1, B2	Candidates + extras	12.7 x 3.81
B3	5 mil Teflon™ FEP/VDA	12.7 x 3.81
G1	Candidates + extras	5.08 x 5.08
L1	Candidates + extras	varied: 15.24 x 12.7 to 25.4 x 20.32

In order to provide a region of stress concentration, each specimen in sets M1, M2, M3, B1, B2 and B3 was sliced through one quarter of its width at a point 5.08 cm from its top. The slices were cut from the inside to the edge of the specimen using a microtome blade. The load used during the radiation exposures was calculated to provide 1000 psi in the net section of the specimen.

Once the specimens were cut they were photographed, and then the test and witness specimens were vacuum baked at 50 °C until the outgassing rate had dropped below the requirements for HST (1.56×10^{-9} g/cm^2/hr). Following bakeout, the solar absorptance was measured, and the specimens were hand-carried to the first exposure site.

3.2 Environmental Exposures Sets of the candidates were exposed to several aspects of the space environment so that the combined effects of the environment could be assessed. In addition to the combined exposures, the effects of thermal cycling and ultraviolet radiation (UV) were evaluated individually. The exposures and set designations are summarized in Table 2. Sample sets were named according to the facility that performed the first exposure. Sets that began with "M" were first exposed at MSFC; "B" sets went to Boeing; "L" sets went to LeRC; and "G" sets remained at GSFC.

TABLE 2: CANDIDATE EXPOSURE SUMMARY

Exposure Set	First Exposure Location	Electron Exposures Duration (years)	Type	Energy (keV)	Proton Energy (keV)	AO (years)	X-ray (years)	Thermal Cycles #	Load	UV (ESH)
M1	MSFC	10	Dose	50 to 500	700	10	-	20,000	taped	-
M2	MSFC	10	Dose	50 to 500	700	-	10	3,200	taped	505
M3	MSFC	6.8	Dose	50 to 500	700	6.8	-	20,000	taped	-
B1	Boeing	10	Fluence	40	40	-	10	1,000	spring	-
B2	Boeing	10	Fluence	40	40	-	-	-	-	-
B3	Boeing	6.8	Fluence	40	40	-	-	-	-	-
L1	LeRC	-	-	-	-	-	-	>1500	mass	-
G1	GSFC	-	-	-	-	-	-	-	-	374
						MSFC	LeRC			GSFC

3.2.1 Combined Environmental Exposures Six sets of specimens (M1, M2, M3, B1, B2, B3) were exposed sequentially to aspects of the space environment at several different facilities.

3.2.1.1 MSFC Exposure Facilities Three environmental elements were simulated at MSFC: electrons, protons and atomic oxygen (AO). During each of these exposures, the specimens were mounted to induce the 1000 psi stress described in section 3.1. The procedure and results of this experiment were detailed in reference 12.

The electron and proton exposures were completed using their Combined Environmental Effects (CEE) test system. The MSFC staff calculated the dose versus depth profile for HST fluences for each candidate. They then designed a fluence of 50 keV, 220 keV and 500 keV electrons and 700 keV protons which matched that profile as closely as possible. During the CEE exposure, the specimens were under vacuum (5×10^{-7} Torr) and were subjected to the electrons of various energies simultaneously and then protons. For all specimens, the exposure times were less than one hour. Specimen sets M1 and M2 were exposed to ten-year HST doses of electrons and protons. Set M3 (the current HST material) was exposed to a SM2-equivalent dose to determine if the observed damage to HST could be duplicated with the test plan (12).

Following electron and proton exposures two sets (M1 and M3) were exposed to atomic oxygen (AO) in their Atomic Oxygen Beam Facility (AOBF). The fluences of the exposures were monitored with control specimens of Kapton® H and pristine Teflon® FEP. The flux was estimated based on measurements of the AO ion current neutralized by the system during a standard run. Set M1 was exposed to a ten-year equivalent HST fluence. Set M3 was exposed to a SM2-equivalent fluence (12).

3.2.1.2 Boeing Exposure Facilities Three material sets were exposed to electron and proton fluences at Boeing Information, Space and Defense Systems, Radiation Effects Laboratory (14). Rather than matching the dose versus depth profile, the Boeing facility matched the total HST fluence of electrons and protons with 40 keV electrons and 40 keV protons. During the exposure the specimens were under load. Sets B1 and B2 were exposed to ten-year HST fluences. Set B3, the current HST material, was exposed to a SM2-equivalent fluence (14). Following this exposure, no further testing was performed on sets B2 and B3 so that they would be available if any tests or simulations were needed in the future.

3.2.1.3 LeRC Exposure Facilities Two types of exposures were completed at LeRC: x-ray exposures and thermal cycling. The x-ray exposures were completed in a chamber equipped with an electron gun and an aluminum target. Flux was measured with a photodiode in a standard run, and the flux value was used to calculate the duration of test runs to achieve the desired fluence. Two sets (M2 and B1) were exposed to ten-year HST-equivalent fluences of Al Kα x-rays. Set B1 was then thermal cycled at LeRC.

The LeRC thermal cycling device was comprised of two thermal chambers dwelling at the two temperature limits, -100 and +50 °C. Specimens were held vertically and raised or lowered from one chamber to the other with a mechanical arm. The cycle time, roughly 5 minutes, was driven by the temperature of an exposed thermocouple. The specimens were spring loaded so that they were stressed throughout the cycle (11). Set B1 received 1000 thermal cycles in this chamber.

3.2.1.3 GSFC Exposure Facilities Rapid thermal cycling and UV exposures were carried out at GSFC. Rapid thermal cycling between -100 °C and +60 °C took place in a modified thermal cycle chamber with a nitrogen purge. Liquid nitrogen vapor and a heat gun were added to the chamber to reduce the period of the cycles to 15 to 20 seconds. Temperatures were monitored with thermocouples taped around the test specimen, and the cycle was driven by a thermocouple affixed with epoxy to a control specimen mounted adjacent to the test specimen (13). Following electron, proton and AO exposures, sets M1 and M3 received 20,000 cycles at GSFC. Set M2 received 3,200 cycles following electron, proton and x-ray exposures.

The GSFC UV exposures were done using a Spectralab X-25 Solar Simulator equipped with a Xenon lamp. The radiation had a minimum wavelength of 180 nm. Following thermal cycling set M2 was exposed to 374 equivalent sun hours (ESH).

3.2.2 Individual Environmental Exposures In addition to the combined effects, the effects of thermal cycling on larger specimens and UV exposure were evaluated.

3.2.2.1 Large Specimen Thermal Cycling Since most of the candidate materials were layered with scrim, concerns were raised about the possibility that thermal cycling could result in permanent deformation of the materials due to mismatched coefficients of thermal expansion or creep properties. The specimens used in the combined effects exposures were too small to address these concerns. Considerably larger specimens (set L1) were thermal cycled at LeRC in order to assess the degree of deformation (10).

Specimens were subjected to at least 1500 cycles with a roughly 9 minute period in the thermal chamber described in section 3.2.1.3. Following the cycles the specimens were evaluated for fractional distortion. Fractional distortion was defined as d/h, where h was the height of the suspended specimen and d was the maximum displacement from true vertical (see Figure 1).

FIGURE 1: FRACTIONAL DISTORTION, d/h (10)

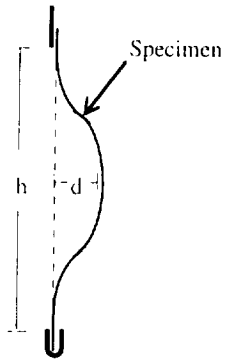

Following thermal cycling, the fractional distortion was calculated for each material. The values are reported in Table 3 (10). The LeRC investigators concluded that shape distortion was a major concern for materials 4 and 7 (10).

TABLE 3: FRACTIONAL DISTORTION (d/h) FROM THERMAL CYCLING (10)

Material #	Initial d/h	Final d/h	Δ	Comments
3	0.020	0.032	0.012	
4	0.008	0.073	0.065	Convex
6	0.020	0.063	0.043	Wavy
7	0.046	0.049	0.003	Concave
8	0.026	0.025	0.001	
9	0.012	0.012	0.000	

3.2.2.2 Ultraviolet Radiation Exposures In order to prove the UV stability of the proprietary adhesives provided by the vendors, the G1 specimens were exposed to ultraviolet radiation and then tested for changes in solar absorptance. The G1 set consisted of two specimens for each candidate material. The specimens were handled vigorously in order to break the metal backing in every specimen so that the UV could reach the adhesive. They were then exposed in the UV chamber (described in section 3.2.1.4) at the beginning of the test plan and remained there as long as possible before the final FRB meeting. Following the meeting, the selected candidate was placed back in the chamber, to determine the maximum value. The pre- and post-exposure solar absorptance values are recorded in Table 4.

4. RESULTS

General observations and absorptance values were recorded before and after each exposure. After the test plan was completed the specimens were sectioned for scanning electron microscope (SEM) analysis of the slice region and the surface.

4.1 General Observations Following the mounting procedure, there appeared to be some evidence of tensile overload at the end of the slice in some specimens. Following electron and proton exposures there were no obvious changes to the specimens, although solar absorptance measurements showed a slight increase (12). Following ten-year AO exposures, the specimens had a matte finish common in AO degradation of materials; this was detected in the solar absorptance measurements (12). No changes were noted after x-ray exposure. Most changes were observed following thermal cycling.

TABLE 4: SOLAR ABSORPTANCE PRE- AND POST-UV EXPOSURE

Material	Sample .#	Solar Absorptance After 374 ESH		
		Initial	Post-UV	Δ
10 mil FEP/VDS/Inconel/adhesive/Nomex	1	0.117, 0.094	0.107, 0.094	-0.010, 0
5 mil FEP/VDS/Inconel/adhesive/ fiberglass scrim/adhesive/Kapton	2	0.082, 0.081	0.080, 0.075	-0.002, -0.006
10 mil FEP/VDA/adhesive Nomex	3	0.164, 0.164	0.174, 0.175	0.010, 0.011
5 mil FEP/VDA/adhesive/fiberglass scrim/adhesive/Kapton	4	0.186, 0.187	0.189, 0.194	0.003, 0.007
5 mil FEP/VDS/Inconel/adhesive/Nomex	5	0.095, 0.086	0.083, 0.083	-0.008, -0.003
5 mil FEP/VDA/adhesive/Nomex	6	0.144, 0.137	0.142, 0.143	-0.002, 0.006
5 mil FEP/VDA	8	0.138, 0.135	0.153, 0.143	0.015, 0.008
$SiO_2/Al_2O_3/Ag/Al_2O_3$/4 mil stainless steel	9	0.074, 0.079	0.079, 0.082	0.005, 0.003
		After 1144 ESH		
5 mil FEP/VDA/adhesive/Nomex	6		0.151, 0.155	0.007, 0.180
$SiO_2/Al_2O_3/Ag/Al_2O_3$/4 mil stainless steel	9		0.094, 0.088	0.020, 0.009

4.1.1 Thermal Cycling Exposure set B1 (electron, proton, x-ray) was cycled while spring loaded at LeRC, and most of the specimens experienced crack growth. Two specimens (B1.2, B1.4) tore in two along the pre-exposure slice before the 1000 cycles were completed, and specimen B1.8 (the current HST material) had torn most of the way across the width by the end of the cycles. Specimens B1.1 and B1.5 had yellowed regions that seemed to be associated with the adhesive.

Exposure sets M1 and M3 experienced 20,000 thermal cycles at GSFC following electron, proton and AO exposure. The specimens appeared dramatically different following thermal cycling. Before cycling, the surface had a diffuse appearance but still seemed mostly transparant; there was no evidence of yellowing. After cycling the materials were milky and the surfaces were nearly opaque. It is believed that the thermal cycling opened micro-cracks at AO erosion trough sites. This appearance change was detected in the solar absorptance measurements. Some specimens also appeared yellowed at the edges; this seemed to be associated with the adhesive. In addition, most of the specimens exhibited some crack propagation.

Set M2 experienced 3,200 thermal cycles at GSFC following electron, proton and x-ray exposure. Several specimens exhibited crack growth. M2.4 delaminated at the interface between the FEP and the VDA, and the crack propagated most of the width of the specimen.

4.2 Solar Absorptance Measurements Before and after each exposure and the total exposure, the solar absorptance was measured. In all cases except following x-ray exposure, the measurements were made with a Laboratory Portable Spectroreflectometer (LPSR). Following the x-ray exposure, the absorptance was measured using a UV-Vis-NIR Spectrophotometer (Perkin-Elmer, Lambda-9). The largest changes in solar absorptance occurred during thermal cycling of exposure set M1. Additional increases were noticed following UV exposure. The final solar absorptance values are reported in Table 5. Solar absorptance measurements were not taken prior to thermal cycling for sets M1, M2, M3. The change in solar absorptance recorded in Table 5 was calculated by subtracting the change from all the other exposures from the overall change. Final measurements were not taken for exposure set B1 before the specimens were sectioned, so the values were estimated by summing the change in solar absorptance from each exposure and the initial measurement.

TABLE 5: CHANGE IN SOLAR ABSORPTANCE ($\Delta\alpha$) FOLLOWING ENVIRONMENTAL EXPOSURES

Sample	Initial α	$\Delta\alpha$ Following Each Exposure					Post Test α	Overall $\Delta\alpha$
		Charged Particles	Atomic Oxygen	X-ray	Thermal Cycling	Near UV		
M1.1	0.092	-0.001	0.017		0.292*	0.039	0.439	0.347
M1.2	0.076	0	0.022		0.007*	0.068	0.173	0.097
M1.3	0.146	0.007	0.030	Not	0.158*	0.071	0.412	0.266
M1.4	0.167	0	0.040	Exposed	0.119*	-0.006	0.320	0.153
M1.5	0.080	0.004	0.025		0.251*	0.029	0.389	0.309
M1.6	0.138	0	0.033		0.083*	0.050	0.304	0.166
M1.8	0.139	0.007	0.024		0.067*	-0.010	0.227	0.088
M2.1	0.093	0		-0.002	0.115*		0.206	0.113
M2.2	0.079	-0.001		-0.003	0.013*		0.088	0.009
M2.3	0.161	0.004	Not	-0.002	0.049*	Not	0.212	0.051
M2.4	0.174	0	Exposed	-0.003	-0.003*	Exposed	0.168	-0.006
M2.5	0.081	0		-0.003	0.042*		0.093	0.012
M2.6	0.140	0		-0.002	0.011*		0.149	0.009
M2.8	0.133	0.002		-0.002	0.039*		0.172	0.039
M3.1	0.139	0.007	0.040	No Exp.	0.061*	.022	0.269	0.130
B1.1	0.087	0.004		0	0.063		0.150*	
B1.2	0.081	-0.002		-0.001	0.003		0.084*	
B1.3	0.152	0.002		0	-0.005		0.147*	
B1.4	0.178	-0.003	Not	0	0.002	Not	0.180*	
B1.5	0.081	0.002	Exposed	0.003	0.037	Exposed	0.118*	
B1.6	0.135	0.002		0	-0.007		0.128*	
B1.7	0.336	0.004		-	-0.001		0.335*	
B1.8	0.135	0.003		-0.004	0.013		0.185*	
B1.9	0.076	0.001		Not	Not			
B1.0	0.172	0.006		Measured	Measured			

* Values calculated rather than measured (see section 4.2)

4.3 Scanning Electron Microscopy (SEM) When all of the exposures were completed, the specimens were sectioned, and SEM analysis was performed. The end of the slice region was analyzed to detect propagation and to study the morphology of the crack. Four basic types of fractures were found: tensile overload (TO), slow crack propagation 1 (SC1), slow crack propagation 2 (SC2), and combinations of TO and slow cracking (TO1 or TO2). The features and causes of these fractures are descibed below, and Table 6 summarizes the type of cracking observed by material and exposure set. Crack extent (length) is addressed in Section 4.3.5 and Table 7.

4.3.1 Tensile Overload (TO) The TO crack surfaces showed plastic deformation with long fibrous tears and thin rippled layers (see Figure 4). This type of failure occurred when the load applied to the specimen, combined with stress concentration at the end of the slice, exceeded the material's ultimate strength while the materials was relatively ductile.

In specimens exposed to AO, the crack surface appeared fibrous. The fibers were oriented in the through-thickness direction and showed little plastic deformation. The AO surface damage appeared to serve as crack-initiating flaws, allowing tensile overload without plastic deformation. The cracks appeared to progress away from the initial notch; the actual crack front tended to move from the AO-exposed surface to the opposite surface.

Evidence of TO was found in specimens B1.1, B1.2, B1.3, B1.4, and B1.7 (see Table 6).

4.3.2 Slow Crack Propagation 1 (SC1) The SC1 crack surfaces were very flat and perpendicular to the specimen surface. There was very little deformation at the specimen surface. The areas between striations were relatively smooth, and there was no evidence of

plastic deformation (see Figure 2). A combination of stress from thermal contraction of the constrained specimen and possible change in material properties during low temperature cycles caused the crack to propagate a short distance. The high temperature portion of the cycle allowed the crack tip to close, therefore the low temperature excursions started with a relatively sharp crack tip. The fracture surface of these cracks most closely resembled those from retrieved HST materials (5).

Evidence of SC1 was found in specimens M1.2, M1.4, M2.3, M2.4, and M2.5 (see Table 6).

4.3.3 Slow Crack Propagation 2 (SC2) The SC2 crack surfaces were wavy, with some deformation at the specimen surface in the direction perpendicular to the specimen surface. Ductile tearing was observed between and at the crests of wavy striations (see Figure 3). As with the SC1, the crack front progressed during thermal cycles. The tension on the specimen was sufficient to cause some plastic deformation. Because the specimen was always under tension, the crack tip did not close with each high temperature excursion. Therefore, low temperature cycles started with a blunted, stressed crack tip.

Evidence of SC2 was found only found in combination with TO (TO2, see Table 6).

4.3.4 Combination (TO1 or TO2) The features of the crack were consistent with single tensile overload adjacent to the initial slit and then changed to either SC1 or SC2 described above. This crack occurred when the initial yielding (TO) reduced the stress concentration below that necessary for failure. The crack then progressed as SC1 or SC2 depending upon the conditions (see Figure 4).

Evidence of TO1 or TO2 was found in specimens M1.5, M2.2, M3.1, B1.5, B1.6, and B1.8 (see Table 6).

TABLE 6: CRACK FEATURES BY CANDIDATE AND SET

Material	Sample .#	Crack Type			
		M1 Set	M2 Set	M3 Set	B1 Set
10 mil FEP/VDS/Inconel/adhesive/Nomex	1	None	None		TO
5 mil FEP/VDS/Inconel/adhesive/ fiberglass scrim/adhesive/Kapton	2	SC1	TO2		TO
10 mil FEP/VDA/adhesive Nomex	3	None	SC1		TO
5 mil FEP/VDA/adhesive/fiberglass scrim/adhesive/Kapton	4	SC1	SC1		TO
5 mil FEP/VDS/Inconel/adhesive/Nomex	5	TO1	SC1		TO1
5 mil FEP/VDA/adhesive/Nomex	6	None	None		TO2
OCLI/White Tedlar	7	-	-		TO
5 mil FEP/VDA	8	TO	None	TO1	TO2
SiO2/Al2O3/Ag/Al2O3/Stainless	9	-	-		None
AZ93 White/Kapton	0	-	-		None

4.3.5 Crack Extent SEM images of the specimens were used to determine how far the cracks propagated from the edge of the pre-exposure slit. Since many of the candidates were layered with different types of scrim, crack length alone was not an effective illustration of the material performance. Table 7 contains descriptive data about the crack propagation in each specimen and each exposure set.

All of the specimens in the B1 exposure set experienced tensile overload. This was most likely caused by the nominal 1000 psi tensile stress during the thermal cycling. Materials in exposure set M2 most frequently experienced slow crack growth similar to the retrieved HST materials.

Specimens with fiberglass scrim (materials 2, 4) experienced the worst cracking. In all test sets these materials showed crack propagation, often accompanied by delamination between the FEP

and the VDA or VDS. In the overly-rigorous load conditions of the B1 exposure set, these materials failed completely.

In specimens with Nomex scrim (materials 1, 3, 5, 6) the crack propagation past the pre-exposure slit stopped before the first or second scrim fiber. Often there was evidence of minor delamination between the FEP and the VDA or VDS.

TABLE 7: CRACK FEATURES BY MATERIAL AND EXPOSURE SET

Material Number	Crack Features					
	M1 Set		M2 Set		B1 Set	
	Type	Extent	Type	Extent	Type	Extent
1	None	-	None	-	TO	to next fiber
2	SC1	delam; long	TO2	short, no delam	TO	tore in two
3	None	-	SC1	short of next fiber	TO	to 2nd fiber
4	SC1	long, no delam	SC1	delam, very long	TO	tore in two
5	TO1	delam; to next fiber	SC1	to 2nd fiber	TO1	to next fiber, delam
6	None	-	None	-	TO2	delam, to next fiber
7	-	-	-	-	TO	long micro crack
8	TO	short	None	-	TO2	mixed, 3/4 of width
9	-		-	-	None	-
0	-		-	-	None	-

5. SELECTION

The FRB used the candidate selection process described in section 2.1 to rank the candidate materials following the environmental exposures. The materials were evaluated based on their performance with respect to each of the nine factors. Two materials, Proprietary Teflon®/AZ93 White Paint/Kapton® (material 0) and $SiO_2/Al_2O_3/Ag/Al_2O_3$/4 mil stainless steel (material 9) were not considered in this final evaluation. Material 0 was eliminated prior to voting because of problems with particulate contamination and UV darkening. The composite coating on stainless steel (material 9) was not practical for the LS repairs in terms of cost or handling. The remaining candidate replacement materials were ranked as in Table 8.

TABLE 8: FINAL RANKING OF CANDIDATE MATERIALS

Rank	Material Number	Material
1	6	5 mil Teflon® FEP /VDA/adhesive/Nomex scrim
2	3	10 mil Teflon® FEP/VDA/adhesive/Nomex® scrim
3	8	5 mil Teflon® FEP/VDA (the current material)
4	1	10 mil Teflon® FEP/VDS/Inconel/adhesive/Nomex® scrim
5	5	5 mil Teflon® FEP/VDS/Inconel/adhesive/Nomex® scrim
6	2	5 mil Teflon® FEP/VDS/Inconel/adhesive/fiberglass scrim/adhesive/2 mil Kapton®
7	7	OCLI multi-layer oxide UV blocker/2 mil white Tedlar®
8	4	5 mil Teflon® FEP/VDA/adhesive/fiberglass scrim/adhesive/2 mil Kapton®

Material 6, (5 mil Teflon® FEP /VDA/non-UV-darkening adhesive/Nomex scrim), was ranked first and recommended as the replacement material for the new outer layer. However, there was some concern that the absorptance value would increase significantly with more UV exposure. Specimen M2.6 was placed back in the UV chamber at GSFC for additional exposure and absorptance measurements. In the event that the recommended material failed this final test, two alternates that had not been included in this test plan were suggested.

The first alternate was $SiO_2/Al_2O_3/Ag/Al_2O_3$/Kapton®. This material had excellent thermal properties, and the coating proved durable in the electron and proton exposures and the large

specimen thermal cycling. The second alternate was unsupported 10 mil Teflon® FEP. This material had the advantage of being commercially available and relatively inexpensive. Also, the 10 mil candidates seemed to perform better in crack resistance than the 5 mil candidates. The project management for HST will make the final selection based on program requirements.

6. CONCLUSION

Based on the nine performance criteria established by the FRB at the beginning of the exposures, material 6 (5 mil Teflon® FEP/VDA/non-UV-darkening adhesive/Nomex scrim) was recommended as the new outer layer for the MLI on the HST LS. The two most important factors in this selection were the optical properties and the structural integrity following the simulated space exposures. Although the absorptance of the selected material did not meet the EOL requirements, it was the best performer among the specimens that maintained structural integrity. Since limited UV exposure was possible during the test plan, UV exposure continues so that the maximum absorptance of this material can be determined before the final decision is made.

Fracture surfaces that resembled those of retrieved HST specimens were observed on several specimens in the M2 exposure set and on two specimens in the M1 exposure set. The highest increase in solar absorptance occured in expsure set M2. Material 1 (10 mil Teflon® FEP/VDS/Inconel/adhesive/Nomex® scrim) had the highest increase in solar absorptance in each exposure set.

7. ACKNOWLEDGMENTS

The staff at the environmental exposure facilities were Dave Edwards (MSFC), Jason Vaughn (MSFC), Dennis Russell (Boeing), Larry Fogdall (Boeing), Kim de Groh (LeRC), Bruce Banks (LeRC) and Wanda Peters (Swales Aerospace). Sample preparation was done by Mary Ayres-Treusdell (GSFC), Tom Zuby (Unisys), and Dave Hughes (Swales Aerospace). Fluence calculations for HST were perfomed by Teri Gregory (Lockheed Martin Technical Operations) and Janet Barth (GSFC).

8. REFERENCES

1) P.A. Hansen, J.A. Townsend, Y. Yoshikawa, J.D. Castro, J.J. Triolo, and W.C. Peters, "Degradation of Hubble Space Telescope Metallized Teflon® FEP Thermal Control Materials", Science of Advanced Materials and Process Engineering Series, 43, 000 (1998).

2) J. A. Townsend, P.A. Hansen, J.A. Dever, J.J. Triolo, "Analysis of Retrieved Hubble Space Telescope Thermal Control Materials", Science of Advanced Materials and Process Engineering Series, 43, 000 (1998).

3) T. Zuby, K. DeGroh, and D. Smith; "Degradation of FEP Thermal Control Materials Returned from the Hubble Space Telescope," NASA Technical Memorandum 104627, December 1995.

4) A. Milintchouk, M. Van Eesbeek, F. Levadou and T. Harper, "Influence of X-ray Solar Flare Radiation on Degradation of Teflon® in Space" Journal of Spacecraft and Rockets, Vol. 34, No. 4, July-August, 1997.

5) L. Wang, J.A. Townsend, and M. Viens, "Fractography of MLI Teflon® FEP from the HST Second Servicing Mission", Science of Advanced Materials and Process Engineering Series, 43, 000 (1998).

6) J.A. Dever, J. A. Townsend, J.R. Gaier and A.I. Jalics, "Synchrotron VUV and Soft X-Ray Radiation Effects on aluminized Teflon® FEP", Science of Advanced Materials and Process Engineering Series, 43, 000 (1998).

7) C. He and J.A. Townsend, "Solar Absorptance of the Teflon® FEP Samples Returned from the HST Servicing Missions", Science of Advanced Materials and Process Engineering Series, 43, 000 (1998).

8) J.A. Dever, K.K. deGroh, J.A. Townsend, L.L. Wang, "Mechanical Properties Degradation of Teflon® FEP Returned from the Hubble Space Telescope", NASA/TM-1998-206618

9) J. Dever, "Summary of HST MLI Materials Analysis Results", NASA Internal Memorandum, June 23, 1997.
10) B. Banks, "Report for 'Potato Chip' Testing of the Candidate HST MLI Replacement Materials", NASA Internal Memorandum, November 21, 1997.
11) B. Banks, T. Stueber, S. Rutledge, D. Jaworske, W. Peters, "Thermal Cycling-Caused Degradation of Hubble Space Telescope Aluminized FEP Thermal Insulation," AIAA 98-0896, Presented at the 36th Aerospace Sciences Meeting & Exhibit, Reno NV, January 12-15, 1998.
12) D.L. Edwards, J.A. Vaughn, *Report on Charged Particle and Atomic Oxygen Exposure of Candidate Replacement Materials for the Hubble Space Telescope (HST)*, October 15, 1997.
13) C. Powers, "Completion of Thermal Cycle Life Tests of HST MLI Samples," NASA Internal Memorandum, January 8, 1998
14) D. Russell, *Test Report "Radiation Exposure Testing -- HST Thermal Blanket,"* November, 1997

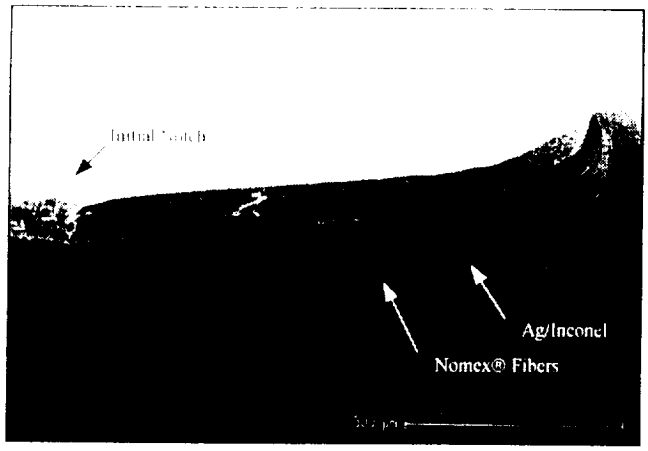

Figure 2a. Specimen M2.5, Entire crack length, including initial razor cut at the far left. Nomex® fibers are revealed behind the crack opening in the center. Silver/Inconel layer is visible at the crack tip to the right.

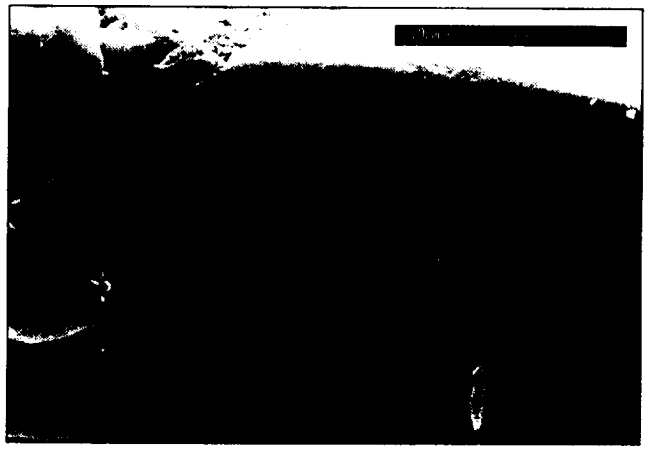

Figure 2b. Specimen M2.5, Initial crack surface, relatively smooth with fine striations.

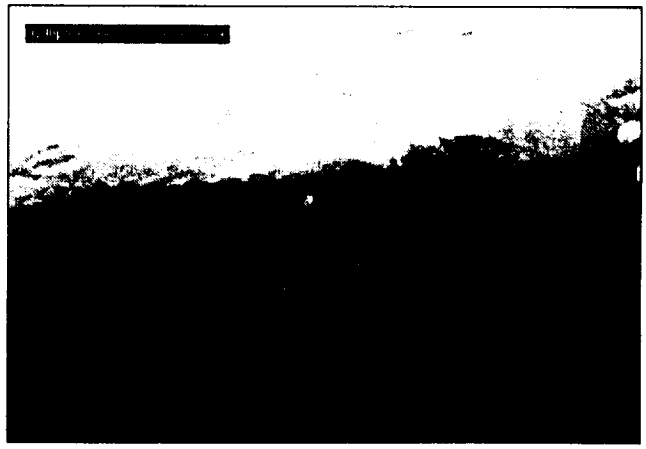

Figure 2c. Specimen 2.5, Detail of striations on the crack surface and the exposed FEP.

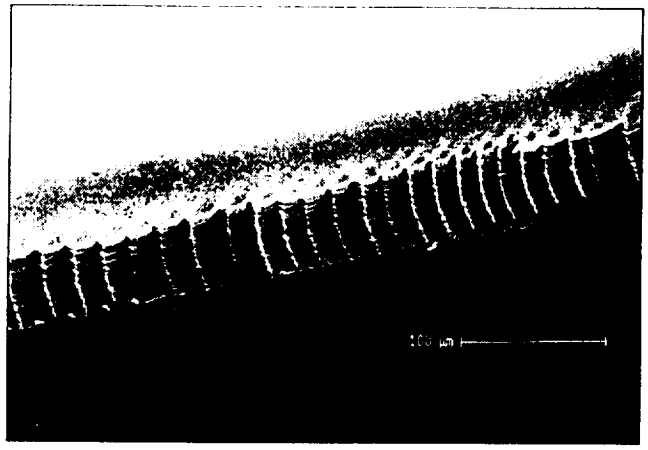

Figure 3a. Specimen B1.8, Five mil FEP with VDA spring loaded during thermal cycling. Shows wave-like striations. Crack propagation was right to left.

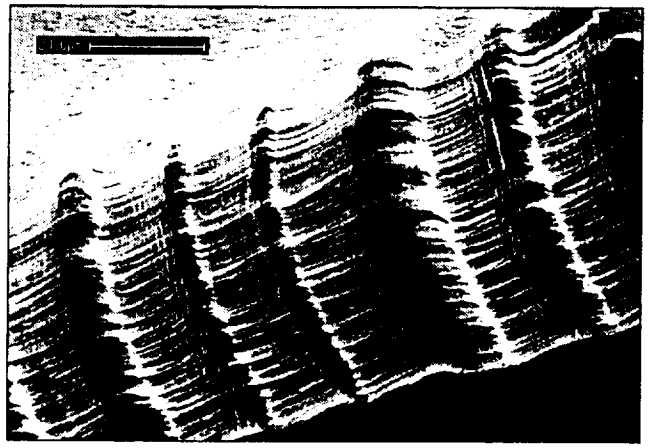

Figure 3b. Detail of the crack surface of specimen B1.8. Crack propagation was right to left.

Figure 3c. Detail of wave-like striations showing ductile tearing features, specimen B1.8.

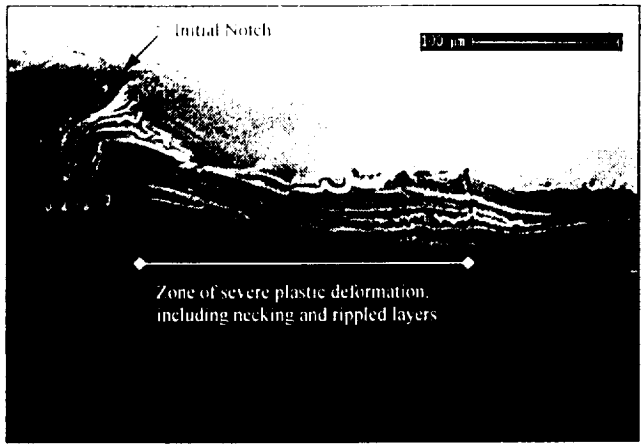

Figure 4a. Specimen B1.6. The initial razor cut is visible at the far left. The crack surface shows significant plastic deformation. Beginning of progressive crack formation is apparent at the far right. Crack propagation was left to right.

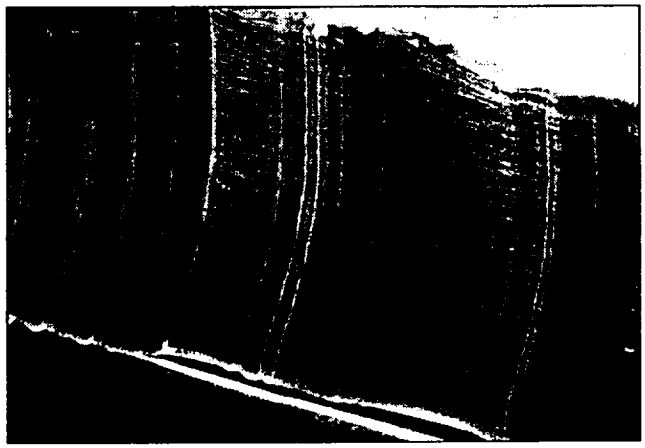

Figure 4b. Specimen B1.6. Midpoint of crack length, crack progression was left to right.

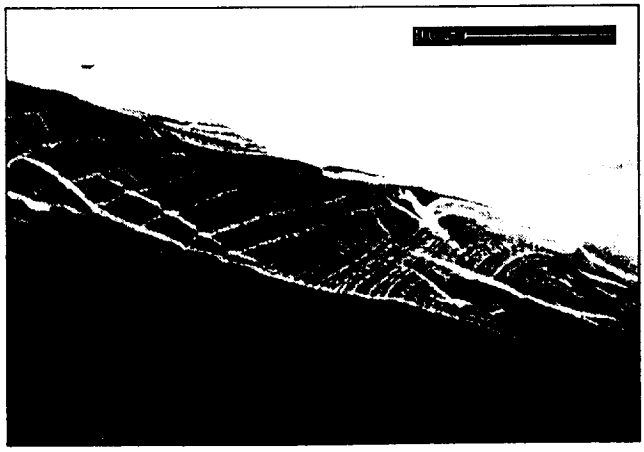

Figure 4c. Specimen B1.6. End of crack. Secondary cracks associated with main crack striations are apparent. Plastic deformation at the extreme right was created during SEM specimen preparation.